Article

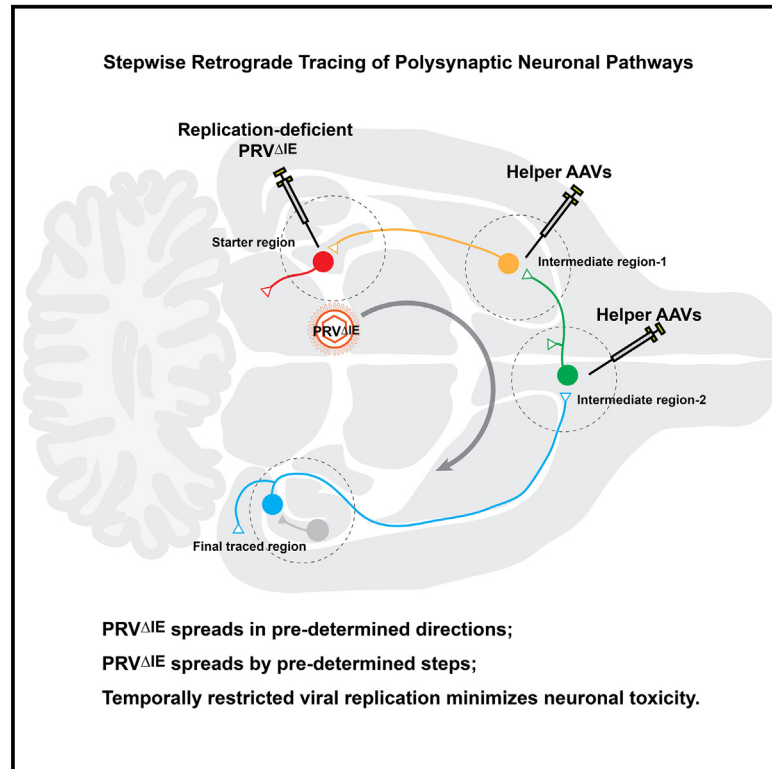# Directed stepwise tracing of polysynaptic neuronal circuits with replication-deficient pseudorabies virus

Graphical abstract

Stepwise Retrograde Tracing of Polysynaptic Neuronal Pathways

Replication-deficient PRV∆IE

Helper AAVs

Starter region

Intermediate region-1

PRV∆IE

Helper AAVs

Intermediate region-2

Final traced region

PRV∆IE spreads in pre-determined directions;
PRV∆IE spreads by pre-determined steps;
Temporally restricted viral replication minimizes neuronal toxicity.

Authors

Wenqin Du, Elizabeth Li, Jun Guo, ..., Ying Li, Hassana K. Oyibo, Wei Xu

Correspondence

wei.xu1@utsouthwestern.edu

In brief

In the brain, information is transmitted and processed by polysynaptic circuits formed by neurons wired together sequentially. Polysynaptic connectivity has been difficult to examine. Here, Du et al. demonstrate that inducible *trans*-complementation of replication-deficient retrograde transneuronal pseudorabies virus (PRV$^{\Delta IE}$) allows continuous tracing of neuronal pathways in a directed and stepwise manner.

Highlights

- Efficient *trans*-complementation of replication-deficient pseudorabies virus

- Stepwise tracing of polysynaptic circuits in a pre-specified direction

- Minimizes neuronal toxicity by temporally restricting viral replication

- Delineates the polysynaptic wiring diagram between hippocampus and striatum

CellPress

Cell Reports Methods

Article

Directed stepwise tracing of polysynaptic neuronal circuits with replication-deficient pseudorabies virus

Wenqin Du,[1,3] Elizabeth Li,[1,3] Jun Guo,[1,3] Rachel Arano,[1] Yerim Kim,[1] Yuh-Tarng Chen,[1] Alyssa Thompson,[1] So Jung Oh,[1] Aspen Samuel,[1] Ying Li,[1] Hassana K. Oyibo,[2] and Wei Xu[1,4,*]
[1]Department of Neuroscience, University of Texas Southwestern Medical Center, Dallas, TX 75390, USA
[2]Friedrich Miescher Institute for Biomedical Research, Basel, Switzerland
[3]These authors contributed equally
[4]Lead contact
*Correspondence: wei.xu1@utsouthwestern.edu
https://doi.org/10.1016/j.crmeth.2023.100506

MOTIVATION The brain is a complex network formed by neurons connected to each other sequentially. To understand its functions, we need to dissect the polysynaptic connectivity of this network. This study develops a tool for tracing the connections in polysynaptic circuits.

SUMMARY

Brain functions are accomplished by polysynaptic circuits formed by neurons wired together through multiple orders of synaptic connections. Polysynaptic connectivity has been difficult to examine due to a lack of methods of continuously tracing the pathways in a controlled manner. Here, we demonstrate directed, stepwise retrograde polysynaptic tracing by inducible reconstitution of replication-deficient *trans*-neuronal pseudorabies virus (PRV$^{\Delta IE}$) in the brain. Furthermore, PRV$^{\Delta IE}$ replication can be temporally restricted to minimize its neurotoxicity. With this tool, we delineate a wiring diagram between the hippocampus and striatum—two major brain systems for learning, memory, and navigation—that consists of projections from specific hippocampal domains to specific striatal areas via distinct intermediate brain regions. Therefore, this inducible PRV$^{\Delta IE}$ system provides a tool for dissecting polysynaptic circuits underlying complex brain functions.

INTRODUCTION

Neurons in the brain connect successively via multiple orders of synapses to form polysynaptic circuits. These polysynaptic circuits encode, process, and transmit information. Delineating the polysynaptic wiring is therefore essential to understanding the neuronal mechanisms underlying brain functions.[1–3] However, it is technically challenging due to a lack of methods of tracking the polysynaptic circuits continuously in a selected direction and passing a pre-determined order of synapses.

Trans-neuronal viruses have been used to map polysynaptic connectivity. A few neurotropic viruses, such as pseudorabies virus (PRV), vesicular stomatitis virus (VSV), rabies virus (RV), and herpes simplex virus (HSV), can replicate in neurons and cross multiple orders of synapses. As self-amplifying tracers, they are powerful tools for tracing polysynaptic circuits.[4–7] However, these replication-competent viruses have significant limitations. Firstly, the viruses are highly toxic and kill the infected neurons and even the animals quickly,[8] making them unsuitable for functional or behavioral analysis. Secondly, the viruses

spread to all connected brain regions and cannot be selectively directed to a particular pathway. Frequently, a large number of brain regions become infected after 2–3 orders of *trans*-neuronal spreading, making it difficult to identify the exact routes the viruses travel on. Thirdly, the viruses may spend different amounts of time spreading across one order of connection depending on the length of axons or other neuronal properties. This makes it hard to determine the sequence of synaptic connections.

Some tracer viruses have recently been modified for monosynaptic tracing. In a pioneering work, glycoprotein was removed from recombinant RV to disable spreading across synapses.[9] *Trans*-neuronal spreading of RV could then be reconstituted by expressing the glycoprotein in *trans*. This allowed monosynaptic inputs to be traced from "starter" neurons that express the glycoprotein.[10] Further engineering of RV made it a versatile tool with broad applications.[11–14] Similar strategies were used to generate recombinant PRV,[15–17] VSV,[18] and HSV.[19,20] This strategy can be combined with other tools to trace circuits spanning three brain regions, albeit the viruses pass only one order of synaptic connection.[21,22]

We reason that the replication or spreading of recombinant viruses can be reconstituted multiple times along a brain circuit to trace polysynaptic pathways. With additional molecular controls built into the *trans*-complementation system, *trans*-neuronal spreading of viruses can also be activated (1) at a desired time, (2) at a selected branch of the circuit, and (3) to pass a pre-determined number of orders of synaptic connections. Recently, we demonstrated that controlled anterograde polysynaptic tracing can be realized by inducible reconstitution of a vaccine for yellow fever, YFV-17D.[23] Here, we used the same strategy to develop a controlled stepwise retrograde tracing method based on PRV. Drawing on the findings that PRV lacking immediate gene IE180 can infect neurons without *trans*-neuronal spreading,[17] we generated adeno-associated virus (AAV) vectors to express a codon-modified optimized IE180 that efficiently reconstituted the replication and *trans*-neuronal transport of PRV. The expression of IE180 was restricted to a short time window to avoid potential neurotoxicity. This system enables us to trace polysynaptic circuits in a directed and stepwise manner. We further used this system to delineate the wiring of the hippocampus-striatum pathways.

RESULTS

Trans-complementation of PRV replication and *trans*-synaptic transport with optimized IE180 (IEo)

PRV is one of the first *trans*-neuronal viruses used for circuit tracing[4,24] and has been modified for a variety of applications.[25,26] PRV has two identical copies of IE180 gene, which is the immediate-early gene expressed right after viral infection to activate viral gene transcription and DNA replication. IE180-null PRV, referred to as PRV$^{\Delta IE}$, can infect neurons but can no longer replicate in neurons or spread across synapses.[15,17] We reason that by expressing IE180 in an inducible manner, we may be able to control the spreading of PRV$^{\Delta IE}$ along brain circuits (Figures 1 and S1).

We use two sets of AAV vectors for inducible expression of IE180: one set (AAV-tTA and AAV-rtTA) expresses the tetracycline-controlled *trans*-activator (tTA) or the reverse tTA (rtTA) under the control of the synapsin promoter,[23] while the other (AAV-TRE-IE180) expresses IE180 under the control of a promoter containing tetracycline-responsive element (TRE) (Figure 1A). tTA activates IE180 expression in the absence of doxycycline (Dox), while rtTA induces IE180 in the presence of Dox. IE180, once expressed, activates the expression of PRV genes and initiates the replication of PRV, which in turn travels across synapses to connected neurons. The PRV strain used in this study lacks the Us9 gene, so it travels in retrograde direction only.[17,27] The PRV$^{\Delta IE}$ carried EGFP or Cre recombinase (Figure S1A). When we infected cultured 3T3 cells or BHK cells (rodent cell lines were chosen because PRV does not infect primate cells) with a high titer of PRV$^{\Delta IE}$-EGFP, expression of EGFP was detected in the cells, indicating that PRV$^{\Delta IE}$ can infect cells without IE180 (Figure S1B). We then titered down PRV$^{\Delta IE}$-EGFP to a level where no EGFP-positive cells were observed when PRV$^{\Delta IE}$-EGFP was the only virus used to infect the cells. We used this condition to test if expression of IE180 could *trans*-complement the replication of PRV$^{\Delta IE}$-EGFP that leads to the

expression of EGFP at a detectable level. We first made an AAV that expresses wild-type IE180 (AAV-TRE-IE^{WT}). We infected cultured 3T3 cells with AAV-tTA and AAV-TRE-IE^{WT} (Figure 1B). 24 h later, a low titer of PRV$^{\Delta IE}$-EGFP was added to the culture medium. To our surprise, addition of AAV-TRE-IE^{WT} did not lead to the appearance of EGFP-positive cells, indicating that these AAVs did not produce efficient *trans*-complementation of PRV$^{\Delta IE}$-EGFP.

The IE180 gene has a GC-rich sequence—80.2% GC—and its GC content of third-codon positions (GC3) is 95.5%, which is higher than the average of 45%–57% in mammals.[28] Codon usage affects gene transcription, translation, and posttranslational folding.[29,30] The functional implication of IE180 codon usage is unknown. High GC content may increase the stability of mRNA and protein expression level.[31] This high GC content, together with two identical copies of IE180, may be a strategy used by PRV to gain a high expression level of IE180 right after infecting host cells to ensure viral replication. In fact, WT IE180 genetically integrated into host cell genome can efficiently *trans*-complement PRV$^{\Delta IE}$.[17] However, in the short genome of AAV (~5 kb), the high GC content of the 4.3 kb IE180 coding sequence may tend to form stable secondary structures that repress its transcription and translation. Therefore, we modified the IE180 coding sequence by lowering its GC content to 61.8% and GC3 to 45% to see if it could improve the efficiency in *trans*-complementation. We name this codon-optimized IE180 IEo and the AAV expressing it AAV-TRE-IEo.

In cultured cells, AAV-TRE-IEo effectively *trans*-complemented PRV$^{\Delta IE}$-EGFP and activated EGFP expression (Figures 1B and S1B). The EGFP-positive cells concentrated in clusters, suggesting that PRV replicated and spread to neighboring cells (Figure S1B). The sensitivity of AAV-TRE-IEo to Dox was tested as well (Figure 1C). No EGFP-positive cells were observed when 1 μg/mL Dox was added to the culture medium 1 h before PRV$^{\Delta IE}$-EGFP infection, suggesting that Dox can completely inhibit PRV$^{\Delta IE}$-EGFP gene expression and replication. Similarly, AAV-rtTA and AAV-TRE-IEo combination led to the formation of EGFP-positive cell clusters only in the presence of Dox (Figure 1D).

We then tested this system *in vivo* with the dentate gyrus (DG)-CA3-septum circuit, where the granule cells in the DG project to CA3 pyramidal cells and the CA3 pyramidal cells further project to the lateral septum (Figure S2). We first examined the transport of a replication-capable PRV expressing EGFP (PRV154) in this pathway (Figures 1E and S2). PRV154 was injected into the septum unilaterally. The brains were fixed 24, 36, or 55 h later, respectively. At 24 h, EGFP-positive cells were mainly confined to the injection site, with sparse distribution in the CA3. At 36 and 55 h, EGFP-positive cells appeared successively in the bilateral CA3 and the DG, confirming the bisynaptic DG-CA3-septum pathway. This demonstrates that WT PRV can be effectively retrogradely transported in this pathway. Next, we examined the transport of PRV$^{\Delta IE}$ in this circuit (Figure 1F). To obtain greater sensitivity, we used PRV$^{\Delta IE}$-Cre in Ai9 mice, whose cells express tdTomato in the presence of Cre.[32] We injected PRV$^{\Delta IE}$-Cre into the septum unilaterally (Figure S2). 2 months later, we observed tdTomato-positive neurons in bilateral CA3 regions
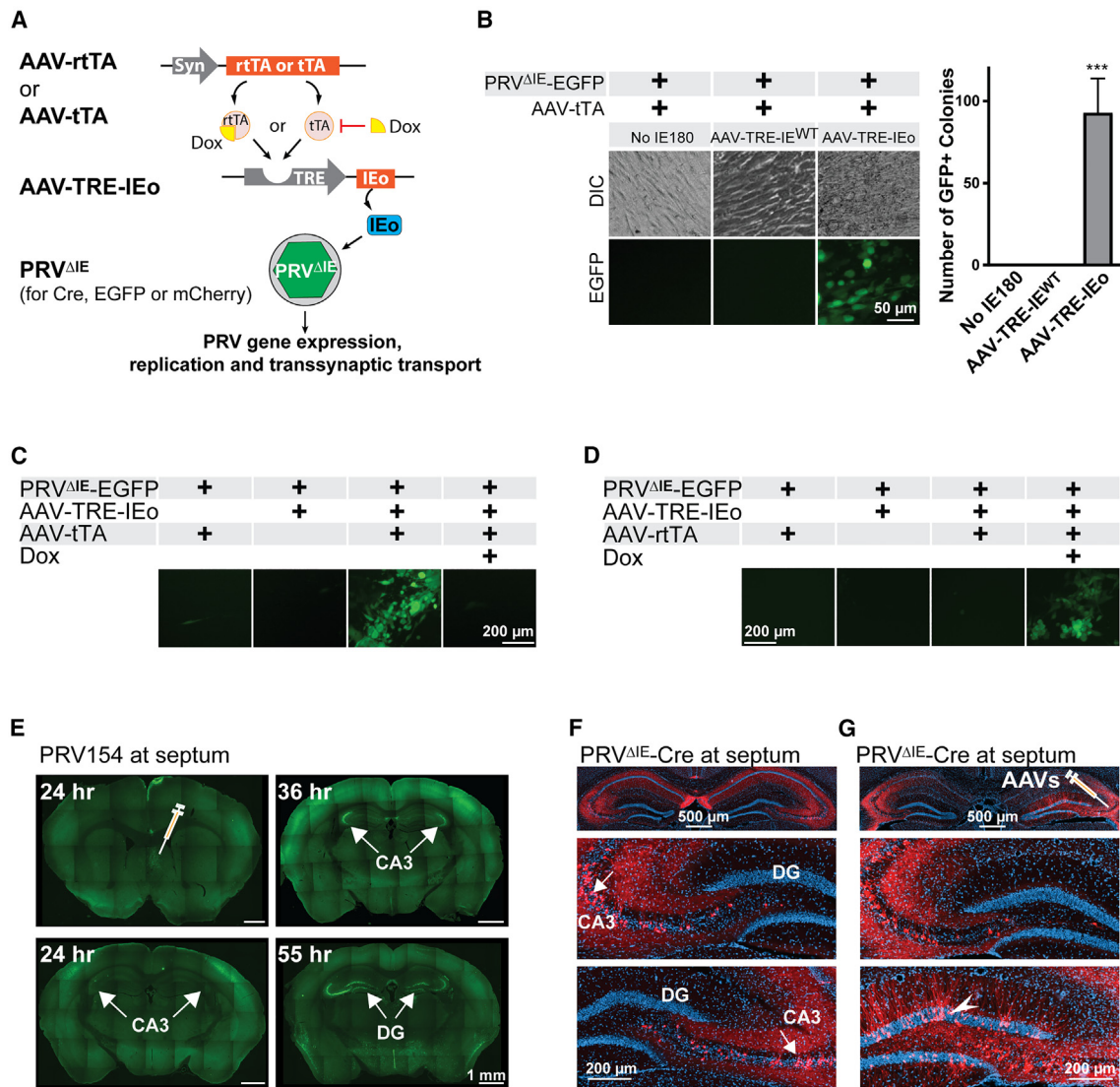
Figure 1. *Trans*-complementation of PRV replication and *trans*-synaptic transport with IEo

(A) AAV vectors (AAV-TRE-IEo and AAV-tTA or AAV–rtTA) were generated for inducible expression of codon-optimized IE180 gene (IEo) to activate the replication of replication-deficient PRV (PRV$^{\Delta IE}$).

(B) Representative photos and quantification showing that the combination of AAV-tTA and AAV-IEo, but not that of AAV-tTA and AAV-IE^{WT} (AAV mediating expression of wild-type IE180), efficiently activated PRV$^{\Delta IE}$-EGFP gene expression and viral replication in cultured 3T3 cells (EGFP expression was quantified by counting GFP+ colonies in each well of 6-well culture plates; the numbers from each batch of experiments were averaged; n = 4 independent experiments. Data are represented as mean ± SEM. ***p < 0.001, Mann-Whitney test).

(C and D) AAV-TRE-IEo and AAV-tTA (C) or AAV-TRE-IEo and AAV-rtTA (D) activated PRV$^{\Delta IE}$ gene expression and viral replication in cultured 3T3 cells in the absence or presence of doxycycline (Dox), respectively.

(E) Replication-capable PRV expressing EGFP (PRV154) was injected into the septum unilaterally. EGFP-positive neurons were detected sequentially in the injection site, the bilateral CA3, and the bilateral dentate gyrus (DG) 24, 36, and 55 h after viral injections, respectively.

(F) PRV$^{\Delta IE}$ expressing Cre (PRV$^{\Delta IE}$-Cre) was unilaterally injected into the septum of tdTomato reporter mice (Ai9 mice). tdTomato-positive neurons were detected at the bilateral CA3 (top panel and enlarged photos in the bottom 2 panels). No tdTomato-positive neurons were detected in the DG contralateral (enlarged photo in the middle panel) or ipsilateral (bottom panel) to the septal injection.

(G) AAV-TRE-IEo and AAV-tTA were co-injected into CA3 unilaterally followed by an injection of PRV$^{\Delta IE}$-Cre in the septum ipsilateral to AAV injection. tdTomato-positive neurons were detected in the bilateral CA3 and in the DG ipsilateral to AAV injections (bottom panel) but not in the contralateral DG (middle panel). See also Figures S1–S3.

but not in the DG, indicating that PRV$^{\Delta IE}$-Cre can be retrogradely transported to the neurons in the CA3 but that, without replication, PRV$^{\Delta IE}$ cannot cross synapses to reach DG, consistent with previous observations.[17]

We then tested if AAVs could restore PRV$^{\Delta IE}$ replication in the brain (Figures 1G and S3). We co-injected AAV-tTA and AAV-IEo into the CA3 unilaterally and 2 weeks later injected PRV$^{\Delta IE}$-Cre into the septum. 3 weeks after PRV$^{\Delta IE}$ injection, we fixed the

brains. Mice drank water containing Dox throughout the experiment starting from AAV injection until perfusion except during the 72 h between 48 h before and 24 h after PRV$^{\Delta IE}$ injection. We observed tdTomato-positive neurons in the DG ipsilateral to CA3 injection, but not in the contralateral DG, indicating that the AAVs effectively activated the replication and retrograde transneuronal transport of PRV$^{\Delta IE}$-Cre from the CA3 to the ipsilateral DG.

Minimizing PRV neuronal toxicity with temporally restricted replication

To determine if PRV$^{\Delta IE}$ produced neuronal toxicity *in vivo*, we quantified the neurons traced in the DG-CA3-septum pathway at different time points (Figures 2A–2D). We first optimized the procedure of pairing AAV-tTA with administering Dox, as shown in Figure 2B. We then perfused mice 7, 14, or 21 days after injecting PRV$^{\Delta IE}$-Cre. The density of traced neurons in the DG increased from day 7 to 14, suggesting that in the final stage of tracing the DG, PRV$^{\Delta IE}$-Cre needs about 2 weeks to reach peak effectiveness in turning on reporter genes. The density of traced neurons did not change from day 14 to 21, indicating no obvious neuronal loss in this time window. Considering that the WT PRV produces neuronal toxicity quickly—within hours to days[33]—the results suggest low neuronal toxicity of PRV$^{\Delta IE}$-Cre.

We also compared the electrophysiological properties of infected neurons with non-infected control neurons (Figure 2E–2I). Here, we used AAV-rtTA to precisely time viral replication. We co-injected AAV-rtTA and AAV-TRE-IEo into the CA3 of Ai9 mice. 2 weeks later, we injected PRV$^{\Delta IE}$-Cre into the contralateral CA1. Mice received an intraperitoneal injections of Dox (50 mg/kg) 18 and 3 h before PRV$^{\Delta IE}$-Cre injection, respectively. 3 weeks later, we prepared acute brain slices containing DG and analyzed them with whole-cell patch clamp recording. tdTomato-positive neurons (infected) and their neighboring non-fluorescent neurons (control) exhibited similar resting membrane potentials, spontaneous synaptic currents, current injection-triggered action potentials, and other electrophysiological properties. We also took confocal images of brain sections from mice receiving the same treatment. Consistent with physiology results, the morphology of the tdTomato-positive neurons appeared normal (Figure 2F). Together, the results indicate that transient replication of PRV$^{\Delta IE}$ does not produce lasting cell toxicity.

Directed stepwise tracing of polysynaptic circuits with PRV$^{\Delta IE}$

In the above tracing from the septum to the DG, PRV traveled along three brain regions but was only transported across one order of synapse. We went on to test if IEo-mediated reconstitution of PRV$^{\Delta IE}$ could be applied multiple times along the circuit to trace polysynaptic connections (Figure 3). We chose a circuit consisting of four brain regions: from the DG to the retrosplenial cortex (RSP) via CA3 and CA1. We used SynaptoTAG2 AAV to examine the direction of synaptic projections along this circuit (Figures 3A, S5, and S6).[23] As shown in Figures 3B–3D, SynaptoTAG2 AAV demonstrated the synaptic projections from the DG to the ipsilateral CA3, from the CA3 to the bilateral CA1, and from the CA1 to the ipsilateral RSP.

We then co-injected AAV-tTA and AAV-IEo into the CA1 and the contralateral CA3 of Ai9 mice, followed by injecting PRV$^{\Delta IE}$-Cre into the ipsilateral RSP 2 weeks later (Figure 3E). The mice drank Dox water except during the 72 h from 48 h before to 24 h after PRV$^{\Delta IE}$-Cre injection. As shown in Figures 3F and 3G, tdTomato-positive neurons were observed in (1) the RSP, the injection site; (2) the ipsilateral CA1, reflecting axonal uptake and unilateral retrograde transport from RSP; (3) the bilateral CA3, due to bilateral *trans*-synaptic transport of PRV$^{\Delta IE}$-Cre from the CA1 to the CA3; and (4) the contralateral DG, due to unilateral *trans*-synaptic transport of PRV$^{\Delta IE}$-Cre from the CA3 to the DG. Therefore, PRV crossed two orders of synaptic connections to reach four brain regions. These results along with Figure 1G indicate that AAV-mediated reconstitution of PRV replication can trace polysynaptic pathways in a pre-determined direction and can pass a pre-determined number of orders of synaptic connections.

We checked if PRV$^{\Delta IE}$ tracing could be confounded by potential retrograde transport of helper AAVs since many serotypes of AAV, including AAV-DJ used in this study, show retrograde uptake by axonal terminals.[34] We injected AAV-tTA in AAV-DJ serotype (AAV-DJ-tTA) into the CA1 to examine if AAV-tTA could be retrogradely transported to the CA3 and enable the spreading of PRV$^{\Delta IE}$ from the septum to the DG (Figures S4A and S4B). We did not observe tdTomato-positive neurons in the DG, suggesting that even if AAV-DJ-tTA was transported from the CA1 to the CA3, it failed to mediate sufficient tTA expression at the CA3 for *trans*-complementation of PRV$^{\Delta IE}$. We also conducted similar experiments by switching AAV-DJ-tTA to AAV-tTA in rAAV2-retro serotype (rAAV2-retro-tTA). rAAV2-retro is an engineered AAV with a high level of retrograde transport.[34] Now, we saw tdTomato-positive neurons in the DG (Figure S4C), indicating that retrogradely transported rAAV2-retro-tTA could enable PRV$^{\Delta IE}$ replication and *trans*-neuronal spreading, albeit with lower efficacy compared with locally injected AAV-tTA (Figure 2C). This property of rAAV2-retro may be combined with PRV$^{\Delta IE}$ for analyzing complex circuits.

Limited direct projections from hippocampus to striatum

After testing in well-characterized neuronal circuits, we used the PRV$^{\Delta IE}$ system to delineate the polysynaptic wiring between the hippocampus and the striatum, two complex brain structures with close functional interactions. We first examined the direct synaptic projection from the hippocampus to the striatum with SynatoTAG2 AAV. When SynatoTAG2 AAV was injected into the dorsal CA1 (Figure 4A) or the CA3 (Figure 4B), no EGFP-positive synapses were detected in either the dorsal striatum or the nucleus accumbens (NAc), although tdTomato-positive axons and EGFP-positive synaptic terminals from the hippocampus could be detected in the neighboring septum (Figures 4A, 4B, S5, and S6). When SynatoTAG2 AAV was injected into the ventral CA1 (some neurons in the adjacent ventral CA3 were also infected), EGFP-positive synaptic terminals were observed in NAc with a concentration in the NAc shell (Figures 4C and S6). The results show that the CA1 or CA3 region in the dorsal hippocampus does not project directly to either the dorsal striatum or the NAc, while the ventral hippocampus projects directly to the
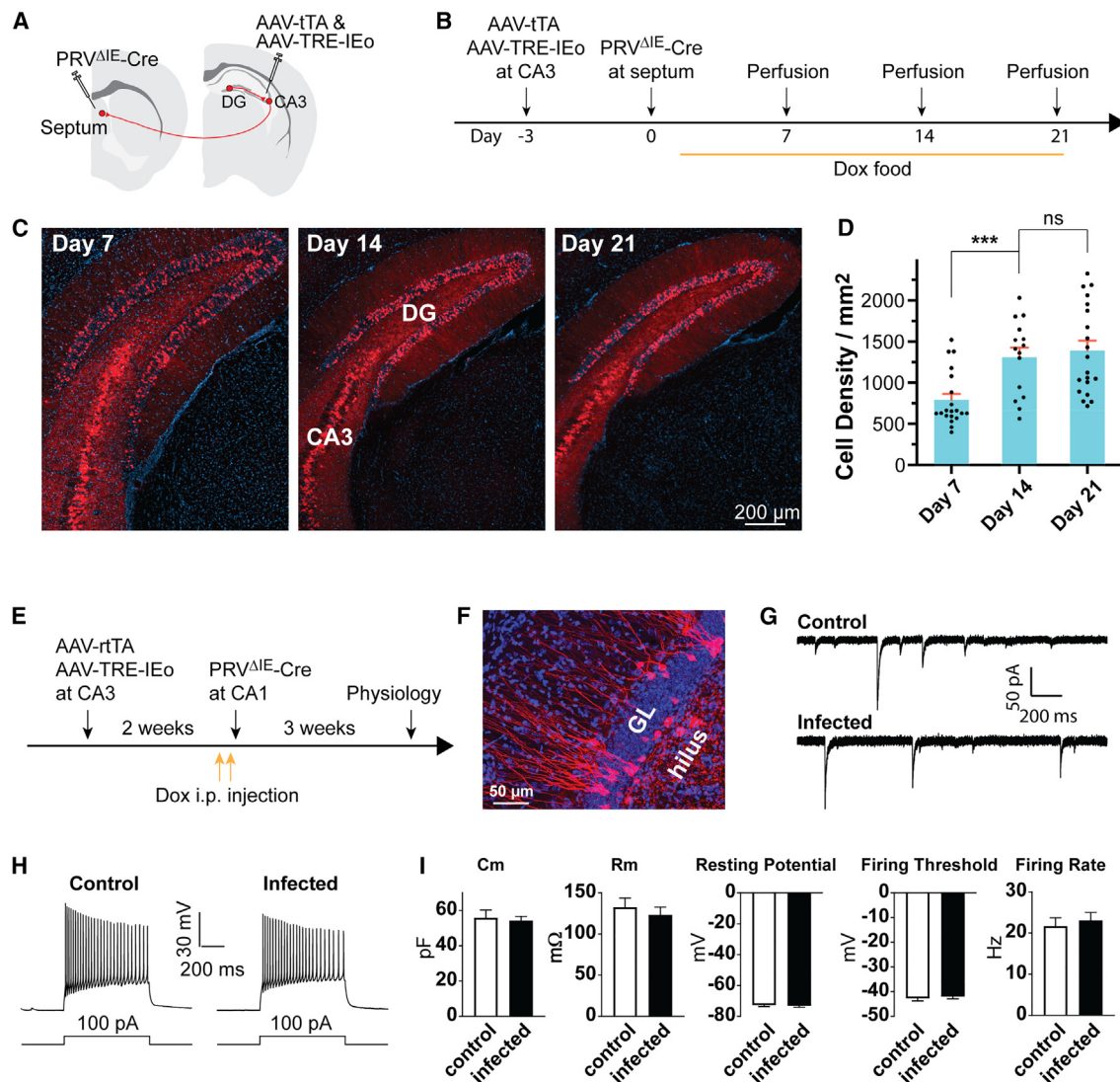
Figure 2. Temporally restricted replication minimized PRV neuronal toxicity

(A–D) Time course of PRV$^{\Delta IE}$-Cre-induced expression of tdTomato.

(A) Schematics showing the DG-CA3-septum pathway.

(B) The time course of viral injections and Dox food and tissue collection.

(C and D) Representative images and quantification of tdTomato-positive cells in the granule layer of the DG in the brains fixed at different time points after the injections of PRV$^{\Delta IE}$-Cre. Data are represented as mean ± SEM. n = 15–20 sections from 3–4 mice in each group. ***p < 0.001, ns indicate p > 0.05 (Mann-Whitney test).

(E–I) Electrophysiological analysis of PRV$^{\Delta IE}$-infected neurons in Ai9 mice.

(E) Time course of viral injections and electrophysiological recordings.

(F) Morphology of tdTomato-positive neurons in DG.

(G and H) Whole-cell patch clamp recordings of tdTomato-positive neurons and their neighboring non-infected control neurons. Both control and PRV$^{\Delta IE}$-Cre-infected neurons demonstrated spontaneous synaptic currents (G) and action potentials triggered by current injections (H).

(I) Quantification of electrophysiological parameters recorded from control and PRV$^{\Delta IE}$-Cre-infected neurons respectively. Cm, membrane capacitance; Rm, membrane resistance. Data are represented as mean ± SEM. n = 14–15 neurons from 3 mice. No statistically significant difference was found between the two groups (Mann-Whitney test, p > 0.05).

See also Figures S3–S4.

NAc but not the dorsal striatum. Consistent with the anterograde tracing with SynatoTAG2 AAV, when PRV$^{\Delta IE}$-Cre alone was injected into the dorsal striatum of Ai9 mice, no tdTomato-positive neurons were found in either the dorsal or the ventral hippocampus (Figure 4D). When PRV$^{\Delta IE}$-Cre alone was injected into the NAc, tdTomato-positive neurons were found in the ventral pole of the ventral hippocampus but not the dorsal hippocampus (Figure 4E).
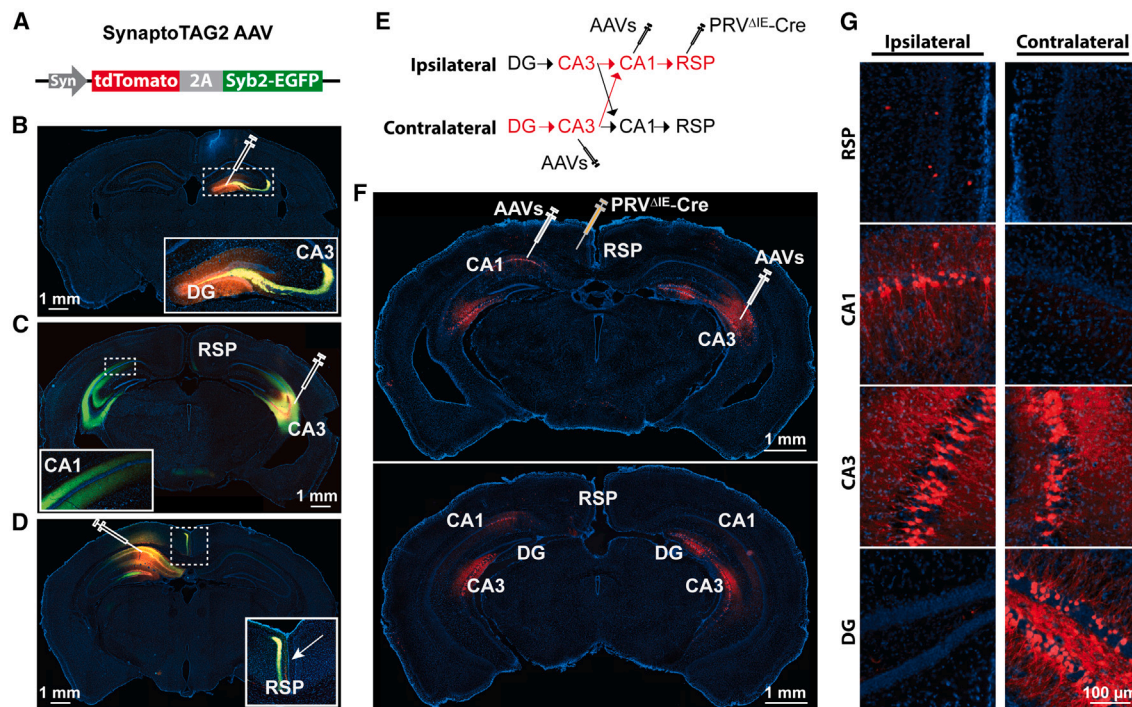
Figure 3. Controlled stepwise tracing of polysynaptic circuits by inducible reconstitution of PRV replication

(A–D) Tracing the synaptic pathways from DG to the retrosplenial area (RSP) with SynaptoTAG2 AAV.

(A) SynaptoTAG2 AAV mediates bicistronic expression of tdTomato (labeling the soma and axons) and EGFP fused to synaptobrevin 2 (Syb2) (labeling synaptic terminals).

(B) DG neurons project to ipsilateral CA3. The insert shows the enlargement of the area marked by dashed lines.

(C) Neurons in CA3 project to bilateral CA1.

(D) Neurons in CA1 project unilaterally to RSP. The arrow points to the midline of the brain.

(E–G) Directed polysynaptic tracing from DG to RSP with PRV$^{\Delta IE}$-Cre.

(E) Schematic showing the injection sites of the AAVs (AAV-tTA and AAV-IEo) and PRV$^{\Delta IE}$-Cre in Ai9 mice. Arrows indicate the direction of synaptic projections.

(F) Two representative brain sections at different anterior-posterior positions showing the directed *trans*-synaptic transport of PRV$^{\Delta IE}$-Cre. tdTomato-positive neurons were detected in the injection site (RSP), the ipsilateral CA1, the bilateral CA3, and the contralateral DG.

(G) Enlargement of the indicated brain regions in (F) (bottom panel).

See also Figure S4.

Tracing polysynaptic projections from the hippocampus to the striatum

We then checked if we could trace the polysynaptic connections between the hippocampus and dorsal striatum by focusing on the prefrontal cortex (PFC) as a potential intermediate region (Figures 5A–5C). Following the protocol in Figure 2B, we injected AAV-tTA and AAV-TRE-IEo into the PFC, AAV-DIO-EGFP into the striatum to label the starting area for PRV tracing, and PRV$^{\Delta IE}$-Cre into the dorsal striatum (Figure 5A). We observed tdTomato-positive neurons in the CA1 region of the intermediate and ventral hippocampus (Figures 5B and 5C), indicating that the expression of IEo in the PFC enabled *trans*-neuronal spreading of PRV from the dorsal striatum to the hippocampus.

We further extended the tracing of the hippocampus-striatum connectivity to substantia nigra pars reticulata (SNr), a downstream target of the striatum. The medium spiny neurons (MSNs) expressing dopamine D1 receptors in the dorsal striatum project to the pars reticulata of the SNr.[35] Here, we injected AAV-tTA and AAV-TRE-IEo into both the dorsal striatum and the PFC for inducible IEo expression and injected PRV$^{\Delta IE}$-Cre into the

SNr (Figure 5D). tdTomato-positive neurons were detected at the SNr, the striatum, the PFC, and the ventral CA1 (Figure 5E). The results indicate that the hippocampus, via the PFC, can innervate the striatal direct pathway. It further demonstrates the effectiveness of this system in elucidating polysynaptic organization of neuronal circuits.

Disynaptic circuits between the hippocampus and dorsal striatum

To systematically trace the hippocampus-dorsal striatum pathways, we picked 6 brain regions receiving direct hippocampal projections to determine if they connect the hippocampus to the striatum (Figure 6). These candidate intermediate brain regions include the PFC, the dorsal subiculum (dSUB), the lateral septum (LS), the entorhinal cortex (EC), the supramammillary nucleus (SUM), and the RSP.[36] We co-injected AAV-rtTA and AAV-TRE-IEo into one of the candidate intermediate brain regions and then injected PRV$^{\Delta IE}$-Cre into the dorsal striatum 2 weeks later. Mice received intraperitoneal injections of Dox (50 mg/kg) 18 and 3 h before PRV$^{\Delta IE}$-Cre injection, respectively.
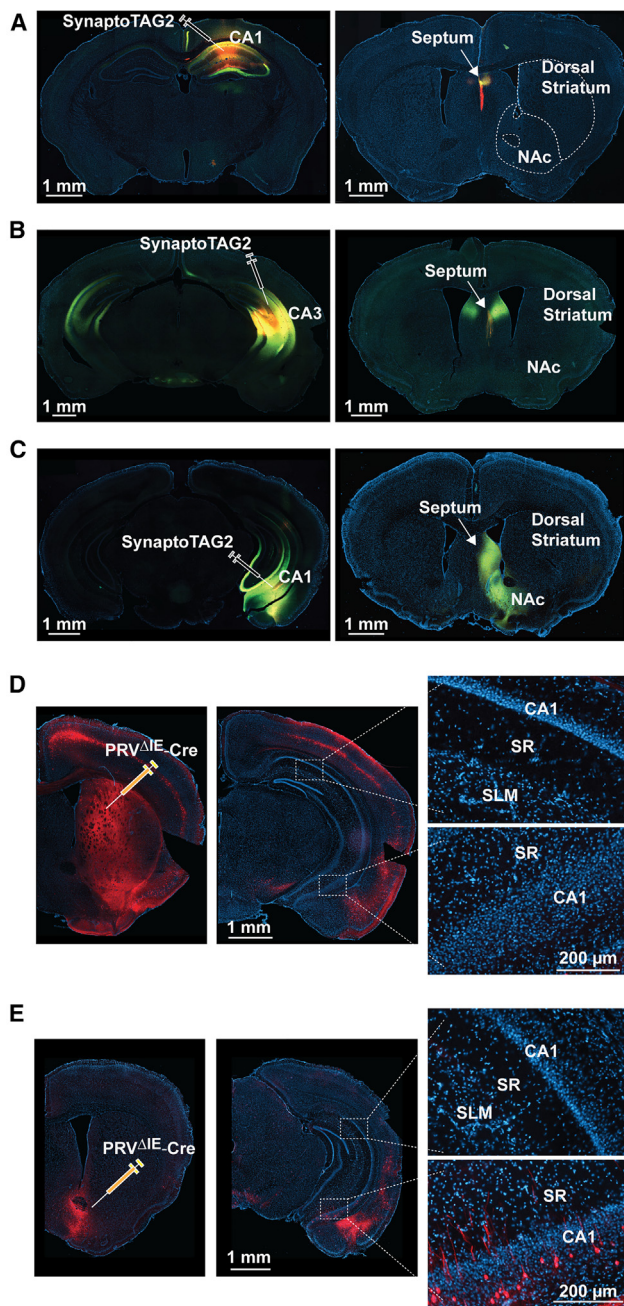
Figure 4. Limited hippocampus-striatum direct projection

(A) SynaptoTAG2 AAV was injected into the dorsal CA1. No EGFP-positive synaptic terminals were observed in the dorsal striatum or the nucleus accumbens (NAc).

(B) SynaptoTAG2 AAV was injected into the CA3.

(C) SynaptoTAG2 AAV was injected into the ventral CA1 (part of the ventral CA3 was also infected). EGFP-positive terminals were in the NAc but not the dorsal striatum. No EGFP-positive synaptic terminals were observed in the dorsal striatum or the NAc.

(D) Ai9 mice received PRV$^{\Delta IE}$-Cre at the dorsal striatum. No tdTomato-positive neurons were observed in the dorsal or ventral hippocampus.

(E) Ai9 mice received PRV$^{\Delta IE}$-Cre at NAc. tdTomato-positive neurons were observed in the ventral but not the dorsal hippocampus.

See also Figures S5 and S6.

The brains were fixed 2 weeks after PRV$^{\Delta IE}$-Cre injection. We observed distinct populations of neurons expressing tdTomato in the dorsal, intermediate, or ventral hippocampus (Figure 6B). When AAVs were injected into the dSUB, tdTomato-positive neurons were detected in the pyramidal cells and interneurons in the dorsal CA1. When AAVs were injected into the PFC, the LS, or the EC, tdTomato-positive pyramidal cells were detected in the intermediate and ventral CA1. When AAVs were injected into the SUM or the rostral part of the RSP (rRSP), we could not detect tdTomato-positive pyramidal cells in the hippocampus, suggesting that the SUM and the rRSP did not provide a bridge connecting the dorsal hippocampus to the dorsal striatum. In the case of dSUB, a significant number of tdTomato-positive pyramidal cells were detected in the CA3 and the DG too, possibly because AAVs diffused to the CA1 and CA3 regions, thus allowing PRV to cross synapses in the hippocampus.

Disynaptic circuits between the hippocampus and the NAc

Similar to the experiments described above, we tested the six brain regions as candidate intermediate brain regions connecting the hippocampal regions to the NAc (Figure 7). We co-injected AAV-rtTA and AAV-IEo into one of the candidate intermediate brain regions of Ai9 mice and injected PRV$^{\Delta IE}$-Cre into the NAc 2 weeks later. Mice received an intraperitoneal injection of Dox (50 mg/kg) 18 and 3 h before PRV$^{\Delta IE}$-Cre injection, respectively. The brains were fixed 2 weeks after PRV$^{\Delta IE}$-Cre injection. When we injected AAVs into the dSUB, we detected tdTomato in the dorsal CA1. When we injected AAVs into the LS, we detected tdTomato-positive neurons in the dorsal CA1 and CA3. PRV$^{\Delta IE}$-Cre traveled to the intermediate and ventral CA1 via the PFC and the EC. When we injected the AAVs into the SUM or rRSP, PRV$^{\Delta IE}$-Cre did not produce tdTomato-positive neurons in the hippocampal areas outside the hippocampal region directly projecting to the NAc (Figure 4E), suggesting that the SUM and the rRSP did not connect the hippocampus to NAc (Figure 7B).

DISCUSSION

Controlled polysynaptic tracing of neuronal circuits

Modern neuroscience started over a century ago when Santiago Ramon Cajal's study of brain histology led to a connectionist view of the neuronal systems: the brain was a network of diverse neuronal cells.[3] Since then, extensive research in neuronal wiring has produced important insights into the brain's structural organization. A large collection of neuronal tracers has been developed including fluorescent proteins, chemicals, and viruses.[1,37–39] *Trans*-neuronal viruses, originally used as self-amplifying tracers, have been modified for monosynaptic tracing. However, we still know little about the long-range polysynaptic circuits and need technologies to probe the polysynaptic neuronal organization. In the current study, we demonstrate that inducible, directed, stepwise tracing of the polysynaptic circuits can be realized with *trans*-complementation of PRV. Here we find that codon-optimized IE180—IEo—significantly improves the efficiency of *trans*-complementation *in vitro* and *in vivo* and that inducible expression of IEo minimizes neuronal toxicity. With this system, viral spreading can be
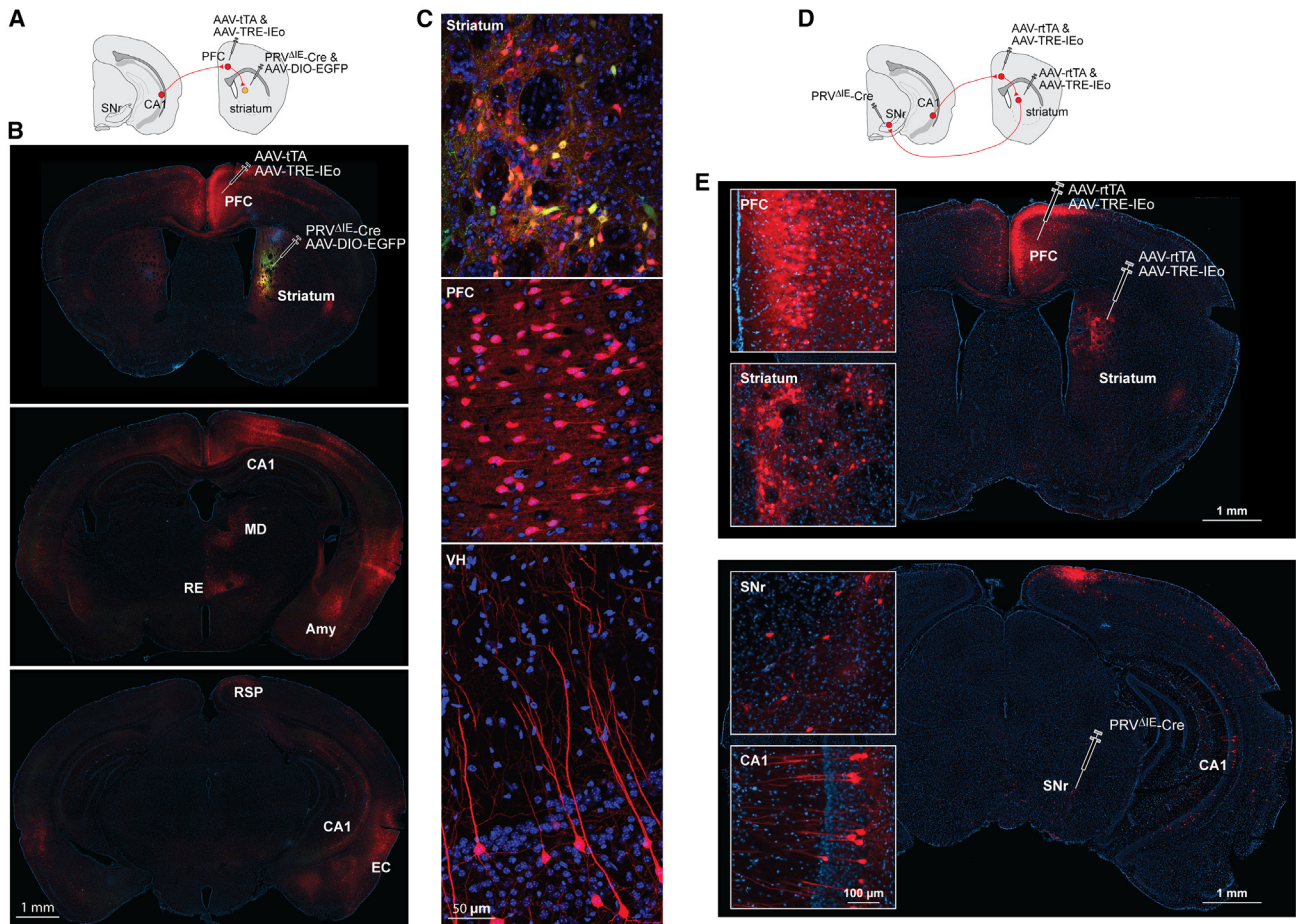
Figure 5. Tracing polysynaptic hippocampus-striatum circuits with PRV$^{\Delta IE}$

(A–C) Tracing hippocampus-PFC-striatum pathway.

(A) Viral injection scheme. Ai9 mice received AAVs (AAV-tTA and AAV-TRE-IEo) at the PFC and PRV$^{\Delta IE}$-Cre at the dorsal striatum. AAV-DIO-EGFP was injected into the striatum to indicate the injection site for PRV$^{\Delta IE}$-Cre.

(B and C) The low- (B) and high-resolution (C) images showing the distribution of tdTomato-positive neurons in the dorsal striatum, the PFC, and the hippocampus, respectively.

(D and E) Tracing tri-synaptic hippocampus-striatum-substantia nigra pars reticulata (SNr) circuits with PRV$^{\Delta IE}$.

(D) Viral injection scheme. Ai9 mice received AAVs (AAV-rtTA and AAV-TRE-IEo) at the dorsal striatum and the PFC and PRV$^{\Delta IE}$-Cre at the SNr.

(B) Representative photos showing tdTomato-positive neurons in the SNr (the PRV$^{\Delta IE}$-Cre injection site), the dorsal striatum (direct presynaptic neuron to SNr neurons), the PFC (the intermediate region), and the CA1 of the hippocampus.

directed to a specific pathway without affecting unintended pathways. We can also determine the number of orders of traced synaptic connections by controlling where IEo is expressed. Furthermore, this system can carry recombinase or other effectors to control or analyze the functions of a specific pathway.

Hippocampus-striatum polysynaptic wiring diagram

The hippocampus and the striatum interact extensively in multiple brain functions. The hippocampus is important for integrating sensory information into representations of the world[40] and for encoding the temporal or spatial relationship among events or objects.[41] The striatum is an interface between the limbic system and motor systems.[42] It plays roles in mediating memory-guided behaviors and motor sequence learning. Both the hippocampus and the striatum have distinct anatomical and functional do-

mains. The hippocampus has prominent functional divisions along its dorsal-ventral, proximal-distal, and superficial-deep axes.[43,44] Similarly, the striatum has a dorsal-ventral division, including the dorsolateral striatum, dorsomedial striatum, and ventral striatum (NAc).[1,45] The dorsolateral striatum is preferentially engaged in procedural learning and stimulus-response learning, the dorsomedial striatum is involved in spatial learning, and the NAc is particularly involved in reinforcement learning. Learning and habit formation require a dynamic interplay of the ventral, dorsomedial, and dorsolateral striatum.[46,47]

Earlier studies of the interactions between the hippocampus and the striatum have focused on the ventral hippocampus and the NAc due to direct connections between the two.[42] The polysynaptic tracing here revealed a few features of the hippocampal projections to the striatum (Figure 7C). (1) The dSUB is
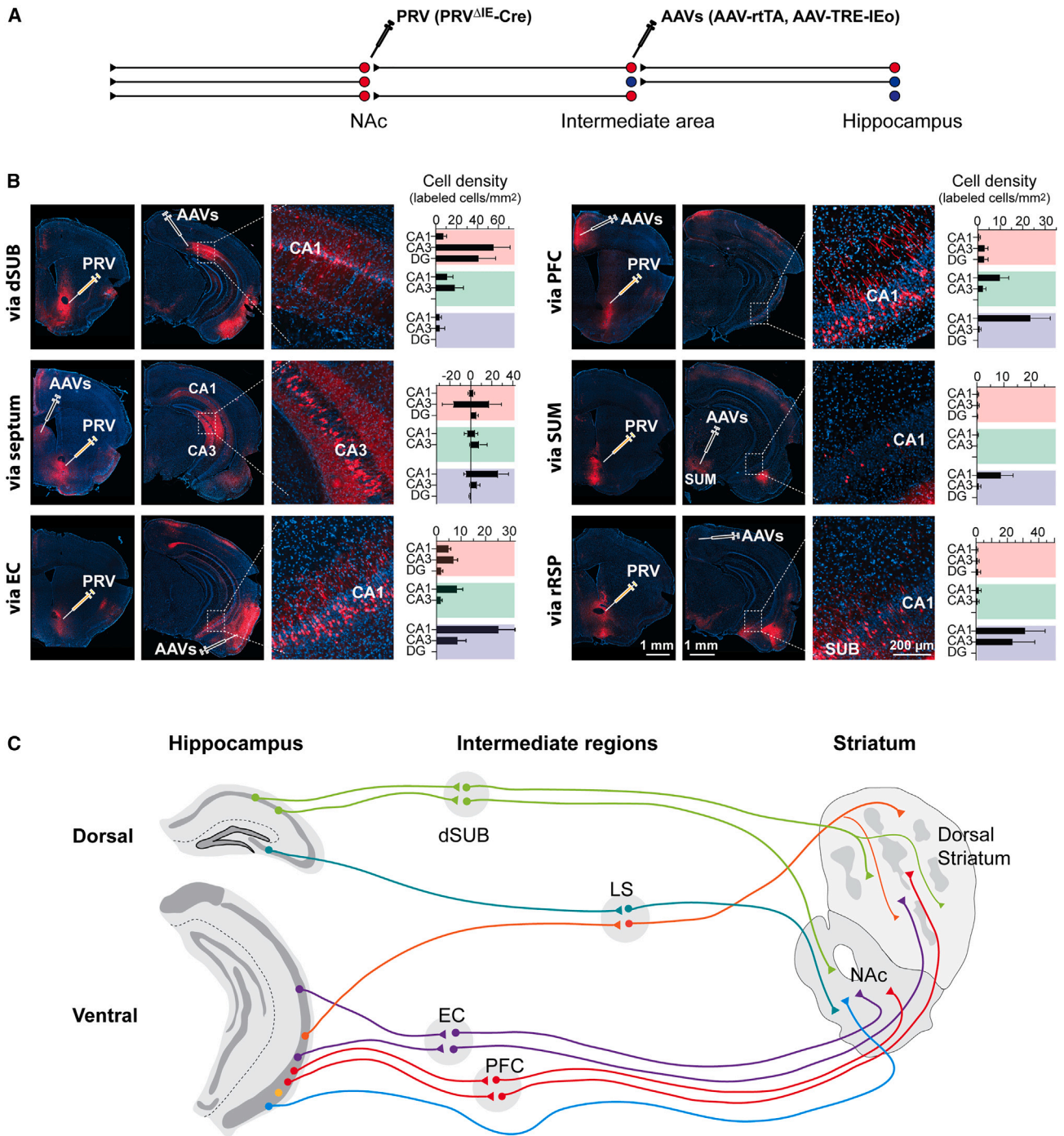
Figure 6. Tracing disynaptic hippocampus-dorsal striatum circuits with PRV$^{\Delta IE}$

(A) Viral injection scheme for directed retrograde tracing of the hippocampus-dorsal striatum circuits. Ai9 mice received AAVs (AAV-rtTA and AAV-IEo) at a selected intermediate region and PRV$^{\Delta IE}$-Cre at the dorsal striatum.

(B) Representative photos and quantification. tdTomato-positive neurons were detected in the dorsal CA1 when PRV$^{\Delta IE}$-Cre passed dSUB. PRV$^{\Delta IE}$-Cre also reached the intermediate and ventral CA1 via the PFC, the septum, and the EC, respectively. SR, stratum radiatum; SLM, stratum lacunosum-moleculare. Data are represented as mean ± SEM. n = 17–33 brain sections from 3–4 mice for each intermediate region. In the bar graphs, positive values indicate that the cells were counted in the hemisphere ipsilateral to the viral injection sides, while the negative values mean that the cells were counted at the hemisphere contralateral to the viral injection sides. tdTomato-positive cells were observed at the contralateral side only when AAVs were injected to the septum. The pink, green, and violet colors denote the dorsal (d), intermediate (i), and ventral hippocampus (v), respectively.

Figure 7. Tracing disynaptic hippocampus-NAc circuits with PRV$^{\Delta IE}$

(A) Viral injection scheme showing the directed retrograde tracing of the hippocampus-NAc circuits with PRV$^{\Delta IE}$-Cre in Ai9 mice. The mice received PRV$^{\Delta IE}$-Cre at the NAc and AAVs (AAV-rtTA and AAV-TRE-IEo) in the indicated intermediate regions, respectively.

(B) Representative photos and quantification showing that tdTomato-positive neurons were detected in different hippocampal regions when AAVs were injected into different intermediate regions. Data are represented as mean ± SEM. n = 29–51 brain sections from 4–6 mice for each intermediate region. In the bar graphs, positive values indicate that the cells were counted in the hemisphere ipsilateral to the viral injection sides, while the negative values mean that the cells were counted at the hemisphere contralateral to viral injection sides.

(C) Schematic summarizing the connectivity revealed in Figures 4, 5, and 6 and this figure.

the major intermediate region for the dorsal CA1 to connect to the dorsal striatum and the NAc. (2) The EC and the PFC are the major regions connecting the ventral CA1 to the dorsal striatum and the NAc. (3) The rRSP does not connect the hippocampus to the striatum, although it receives dense inputs from the CA1 (Figure 3D). (4) The SUM does not connect the dorsal CA1 to the NAc, although the dorsal CA1 sends dense inputs to the SUM (Figure S6A) and the SUM neurons project to the NAc (Figure 7B, SUM panel). (5) The LS connects the dorsal CA1 and CA3 to the NAc and connects the ventral CA1 to the dorsal striatum. (6) Most connectivity is unilateral except that the LS connects the striatum to the hippocampus in both hemispheres. (7) Tracing of the hippocampus-SNr polysynaptic pathway indicates that the direct pathway of the dorsal striatum can be innervated by the hippocampus through CA1-PFC projections.

These data are consistent with early tracing studies in that ventral hippocampus and the dSUB, but not the dorsal CA1, project to the NAc.[48–52] In a recent study, the dorsal CA1 was found to project to the NAc with local AAV infection.[53] However, we did not observe these projections with either anterograde or retrograde tracing. Considering that the subiculum is right next to the CA1 and that AAVs tend to spread to large areas, it is possible these NAc-projecting fibers actually originated from the dSUB. Here, with this PRV$^{\Delta IE}$ system, we delineated the polysynaptic wiring diagram from the hippocampus to the striatum. The results demonstrate that specific anatomical domains in the hippocampus are connected to specific anatomical domains in the striatum via distinct intermediate brain regions.

These separate tracts may organize neurons in multiple regions into distinct functional channels, and each channel may selectively process one type of information. Therefore, this wiring diagram may provide a road map for elucidating the hippocampus-striatum interaction in normal brain functions and diseases. For example, exposure to contextual cues related to previous drug use may trigger relapse in drug abuse.[54] The dorsal hippocampus is critical for contextual memory, while the striatum is the key region for compulsive drug use. The dSUB and the septum are the major brain regions linking the dorsal hippocampus to the striatum and therefore are the candidate regions to mediate this context-drug use association. In another example, patients with schizophrenia exhibit significant alterations in the anterior hippocampus (corresponding to the ventral hippocampus in rodents),[55] and they frequently demonstrate locomotion symptoms that are closely related to dorsal striatal functions.[56] The multiple regions linking the ventral hippocampus to the dorsal striatum are therefore candidates for mediating this interaction. Since the PRV$^{\Delta IE}$-Cre system can turn on or off the expression of genes, we can use it to express in the selected pathways specific tools for functional manipulations, such as optogenetics or chemogenetic tools. These manipulations will allow us to determine the functions of the specific functional channel between the hippocampus and the striatum.

Limitations of the study

The current inducible PRV system does have some limitations and will require further improvements for even broader applications. (1) Tracing from specific neuronal types: the current system is used to study the wiring among brain regions. To study the connectivity of specific neuronal cell types, we will need to make the IEo expression conditional. Due to the large size of the IEo protein, significant optimizations may be needed to make conditional AAV vectors carrying IEo. An alternative strategy will be to render the tTA or rtTA conditional. (2) Spreading in local circuits: with the current PRV system, we cannot exclude the possibility that PRV replicates and spreads via local interneurons in each of the intermediate regions. This local spreading may confound the results. If we can restrict PRV replication to a specific type of neurons, we can minimize this possibility. (3) Complexity in experiments: the IE180 gene needs to be turned on before or at the time of PRV injection to enable *trans*-neuronal spreading. Therefore, the AAVs encoding IE180 need to be injected before PRV injection. As mentioned earlier, in the absence of IE180 PRV may be more vulnerable to host defense.[15] Temporarily inhibiting neuronal antiviral machinery may allow us to inject the PRV$^{\Delta IE}$ and the helper AAVs together. (4) Dependence on reporter mouse lines: among the IE180-null PRVs, PRV$^{\Delta IE}$-Cre performs the best in neuronal tracing. We need to apply it to reporter mice to trace at the whole-brain level (though reporter AAV can be used in combination with PRV$^{\Delta IE}$-Cre, it does not provide connectivity information at the whole-brain level). (5) Difficulty in visualizing IE180 expression in the brain: IE180 is a large gene with a 4.3 kb coding sequence. Due to the size limit of AAVs, we cannot add a fluorescent protein in AAV-TRE-IEo. Generating an antibody of IE180 for immunohistochemistry may help to overcome this limitation. Furthermore, PRV does not infect primates, making it not suitable for studying primates.

STAR★METHODS

Detailed methods are provided in the online version of this paper and include the following:

- KEY RESOURCES TABLE
- RESOURCE AVAILABILITY
  - Lead contact
  - Materials availability
  - Data and code availability
- EXPERIMENTAL MODEL AND STUDY PARTICIPANT DETAILS
  - Mice
  - Cell culture
- METHOD DETAILS
  - Viral vector construction
  - Virus production
  - Stereotaxic viral injection
  - Doxycycline administration
  - Histological analysis
  - Brain slice electrophysiology recording
- QUANTIFICATION AND STATISTICAL ANALYSIS

SUPPLEMENTAL INFORMATION

Supplemental information can be found online at https://doi.org/10.1016/j.crmeth.2023.100506.

AUTHOR CONTRIBUTIONS

W.X. designed and supervised this study. W.D., E.L., J.G., Y.K., R.A., Y.-t.C., A.T., S.J.O., A.S., and Y.L. generated the AAV vectors and conducted the experiments. H.K.O. provided PRV vectors and instructions on packaging/use of PRV vectors. All authors participated in writing.

DECLARATION OF INTERESTS

The authors declare no competing interests.

INCLUSION AND DIVERSITY

One or more of the authors of this paper self-identifies as an underrepresented ethnic minority in their field of research or within their geographical location. One or more of the authors of this paper self-identifies as a gender minority in their field of research. We worked to ensure diversity in experimental samples through the selection of the cell lines.

REFERENCES

1. Foster, N.N., Barry, J., Korobkova, L., Garcia, L., Gao, L., Becerra, M., Sherafat, Y., Peng, B., Li, X., Choi, J.H., et al. (2021). The mouse cortico-basal ganglia-thalamic network. Nature *598*, 188–194. https://doi.org/10.1038/s41586-021-03993-3.

2. Zeng, H., and Sanes, J.R. (2017). Neuronal cell-type classification: challenges, opportunities and the path forward. Nat. Rev. Neurosci. *18*, 530–546. https://doi.org/10.1038/nrn.2017.85.

3. Swanson, L.W., and Lichtman, J.W. (2016). From cajal to connectome and beyond. Annu. Rev. Neurosci. *39*, 197–216. https://doi.org/10.1146/annurev-neuro-071714-033954.

4. Card, J.P., Whealy, M.E., Robbins, A.K., Moore, R.Y., and Enquist, L.W. (1991). Two alpha-herpesvirus strains are transported differentially in the rodent visual system. Neuron *6*, 957–969.

5. Lundh, B. (1990). Spread of vesicular stomatitis virus along the visual pathways after retinal infection in the mouse. Acta Neuropathol. *79*, 395–401.

6. Astic, L., Saucier, D., Coulon, P., Lafay, F., and Flamand, A. (1993). The CVS strain of rabies virus as transneuronal tracer in the olfactory system of mice. Brain Res. *619*, 146–156.

7. Blessing, W.W., Ding, Z.Q., Li, Y.W., Gieroba, Z.J., Wilson, A.J., Hallsworth, P.G., and Wesselingh, S.L. (1994). Transneuronal labelling of CNS neurons with herpes simplex virus. Prog. Neurobiol. *44*, 37–53.

8. Enquist, L.W. (2002). Exploiting circuit-specific spread of pseudorabies virus in the central nervous system: insights to pathogenesis and circuit tracers. J. Infect. Dis. *186*, S209–S214. https://doi.org/10.1086/344278.

9. Wickersham, I.R., Finke, S., Conzelmann, K.K., and Callaway, E.M. (2007). Retrograde neuronal tracing with a deletion-mutant rabies virus. Nat. Methods *4*, 47–49. https://doi.org/10.1038/nmeth999.

10. Wickersham, I.R., Lyon, D.C., Barnard, R.J.O., Mori, T., Finke, S., Conzelmann, K.K., Young, J.A.T., and Callaway, E.M. (2007). Monosynaptic restriction of transsynaptic tracing from single, genetically targeted neurons. Neuron *53*, 639–647. https://doi.org/10.1016/j.neuron.2007.01.033.

11. Chatterjee, S., Sullivan, H.A., MacLennan, B.J., Xu, R., Hou, Y., Lavin, T.K., Lea, N.E., Michalski, J.E., Babcock, K.R., Dietrich, S., et al. (2018). Nontoxic, double-deletion-mutant rabies viral vectors for retrograde targeting of projection neurons. Nat. Neurosci. *21*, 638–646. https://doi.org/10.1038/s41593-018-0091-7.

12. Ciabatti, E., González-Rueda, A., Mariotti, L., Morgese, F., and Tripodi, M. (2017). Life-long genetic and functional access to neural circuits using self-inactivating rabies virus. Cell *170*, 382–392.e14. https://doi.org/10.1016/j.cell.2017.06.014.

13. Reardon, T.R., Murray, A.J., Turi, G.F., Wirblich, C., Croce, K.R., Schnell, M.J., Jessell, T.M., and Losonczy, A. (2016). Rabies virus CVS-N2c(DeltaG) strain enhances retrograde synaptic transfer and neuronal viability. Neuron *89*, 711–724. https://doi.org/10.1016/j.neuron.2016.01.004.

14. Osakada, F., Mori, T., Cetin, A.H., Marshel, J.H., Virgen, B., and Callaway, E.M. (2011). New rabies virus variants for monitoring and manipulating activity and gene expression in defined neural circuits. Neuron *71*, 617–631. https://doi.org/10.1016/j.neuron.2011.07.005.

15. Wu, B.W., Engel, E.A., and Enquist, L.W. (2014). Characterization of a replication-incompetent pseudorabies virus mutant lacking the sole immediate early gene IE180. mBio *5*, e01850. https://doi.org/10.1128/mBio.01850-14.

16. Kondoh, K., Lu, Z., Ye, X., Olson, D.P., Lowell, B.B., and Buck, L.B. (2016). A specific area of olfactory cortex involved in stress hormone responses to predator odours. Nature *532*, 103–106. https://doi.org/10.1038/nature17156.

17. Oyibo, H.K., Znamenskiy, P., Oviedo, H.V., Enquist, L.W., and Zador, A.M. (2014). Long-term Cre-mediated retrograde tagging of neurons using a novel recombinant pseudorabies virus. Front. Neuroanat. *8*, 86. https://doi.org/10.3389/fnana.2014.00086.

18. Beier, K.T., Saunders, A.B., Oldenburg, I.A., Sabatini, B.L., and Cepko, C.L. (2013). Vesicular stomatitis virus with the rabies virus glycoprotein directs retrograde transsynaptic transport among neurons in vivo. Front. Neural Circ. *7*, 11. https://doi.org/10.3389/fncir.2013.00011.

19. Zeng, W.B., Jiang, H.F., Gang, Y.D., Song, Y.G., Shen, Z.Z., Yang, H., Dong, X., Tian, Y.L., Ni, R.J., Liu, Y., et al. (2017). Anterograde monosynaptic transneuronal tracers derived from herpes simplex virus 1 strain H129. Mol. Neurodegener. *12*, 38. https://doi.org/10.1186/s13024-017-0179-7.

20. Lo, L., and Anderson, D.J. (2011). A Cre-dependent, anterograde transsynaptic viral tracer for mapping output pathways of genetically marked neurons. Neuron *72*, 938–950. https://doi.org/10.1016/j.neuron.2011.12.002.

21. Schwarz, L.A., Miyamichi, K., Gao, X.J., Beier, K.T., Weissbourd, B., DeLoach, K.E., Ren, J., Ibanes, S., Malenka, R.C., Kremer, E.J., and Luo, L. (2015). Viral-genetic tracing of the input-output organization of a central noradrenaline circuit. Nature *524*, 88–92. https://doi.org/10.1038/nature14600.

22. Xu, C., Krabbe, S., Gründemann, J., Botta, P., Fadok, J.P., Osakada, F., Saur, D., Grewe, B.F., Schnitzer, M.J., Callaway, E.M., and Lüthi, A. (2016). Distinct hippocampal pathways mediate dissociable roles of context in memory retrieval. Cell *167*, 961–972.e16. https://doi.org/10.1016/j.cell.2016.09.051.

23. Li, E., Guo, J., Oh, S.J., Luo, Y., Oliveros, H.C., Du, W., Arano, R., Kim, Y., Chen, Y.T., Eitson, J., et al. (2021). Anterograde transneuronal tracing and genetic control with engineered yellow fever vaccine

YFV-17D. Nat. Methods *18*, 1542–1551. https://doi.org/10.1038/s41592-021-01319-9.

24. Ekstrand, M.I., Enquist, L.W., and Pomeranz, L.E. (2008). The alpha-herpesviruses: molecular pathfinders in nervous system circuits. Trends Mol. Med. *14*, 134–140. https://doi.org/10.1016/j.molmed.2007.12.008.

25. Pomeranz, L.E., Ekstrand, M.I., Latcha, K.N., Smith, G.A., Enquist, L.W., and Friedman, J.M. (2017). Gene expression profiling with cre-conditional pseudorabies virus reveals a subset of midbrain neurons that participate in reward circuitry. J. Neurosci. *37*, 4128–4144. https://doi.org/10.1523/JNEUROSCI.3193-16.2017.

26. DeFalco, J., Tomishima, M., Liu, H., Zhao, C., Cai, X., Marth, J.D., Enquist, L., and Friedman, J.M. (2001). Virus-assisted mapping of neural inputs to a feeding center in the hypothalamus. Science *291*, 2608–2613. https://doi.org/10.1126/science.1056602.

27. Kratchmarov, R., Taylor, M.P., and Enquist, L.W. (2013). Role of Us9 phosphorylation in axonal sorting and anterograde transport of pseudorabies virus. PLoS One *8*, e58776. https://doi.org/10.1371/journal.pone.0058776.

28. Romiguier, J., Ranwez, V., Douzery, E.J.P., and Galtier, N. (2010). Contrasting GC-content dynamics across 33 mammalian genomes: relationship with life-history traits and chromosome sizes. Genome Res. *20*, 1001–1009. https://doi.org/10.1101/gr.104372.109.

29. Liu, Y. (2020). A code within the genetic code: codon usage regulates co-translational protein folding. Cell Commun. Signal. *18*, 145. https://doi.org/10.1186/s12964-020-00642-6.

30. Zhou, Z., Dang, Y., Zhou, M., Li, L., Yu, C.H., Fu, J., Chen, S., and Liu, Y. (2016). Codon usage is an important determinant of gene expression levels largely through its effects on transcription. Proc. Natl. Acad. Sci. USA *113*, E6117–E6125. https://doi.org/10.1073/pnas.1606724113.

31. Kudla, G., Lipinski, L., Caffin, F., Helwak, A., and Zylicz, M. (2006). High guanine and cytosine content increases mRNA levels in mammalian cells. PLoS Biol. *4*, e180. https://doi.org/10.1371/journal.pbio.0040180.

32. Madisen, L., Zwingman, T.A., Sunkin, S.M., Oh, S.W., Zariwala, H.A., Gu, H., Ng, L.L., Palmiter, R.D., Hawrylycz, M.J., Jones, A.R., et al. (2010). A robust and high-throughput Cre reporting and characterization system for the whole mouse brain. Nat. Neurosci. *13*, 133–140. https://doi.org/10.1038/nn.2467.

33. McCarthy, K.M., Tank, D.W., and Enquist, L.W. (2009). Pseudorabies virus infection alters neuronal activity and connectivity in vitro. PLoS Pathog. *5*, e1000640. https://doi.org/10.1371/journal.ppat.1000640.

34. Tervo, D.G.R., Hwang, B.Y., Viswanathan, S., Gaj, T., Lavzin, M., Ritola, K.D., Lindo, S., Michael, S., Kuleshova, E., Ojala, D., et al. (2016). A designer AAV variant permits efficient retrograde access to projection neurons. Neuron *92*, 372–382. https://doi.org/10.1016/j.neuron.2016.09.021.

35. Calabresi, P., Picconi, B., Tozzi, A., Ghiglieri, V., and Di Filippo, M. (2014). Direct and indirect pathways of basal ganglia: a critical reappraisal. Nat. Neurosci. *17*, 1022–1030. https://doi.org/10.1038/nn.3743.

36. Cenquizca, L.A., and Swanson, L.W. (2007). Spatial organization of direct hippocampal field CA1 axonal projections to the rest of the cerebral cortex. Brain Res. Rev. *56*, 1–26. https://doi.org/10.1016/j.brainresrev.2007.05.002.

37. Bienkowski, M.S., Bowman, I., Song, M.Y., Gou, L., Ard, T., Cotter, K., Zhu, M., Benavidez, N.L., Yamashita, S., Abu-Jaber, J., et al. (2018). Integration of gene expression and brain-wide connectivity reveals the multi-scale organization of mouse hippocampal networks. Nat. Neurosci. *21*, 1628–1643. https://doi.org/10.1038/s41593-018-0241-y.

38. Viswanathan, S., Williams, M.E., Bloss, E.B., Stasevich, T.J., Speer, C.M., Nern, A., Pfeiffer, B.D., Hooks, B.M., Li, W.P., English, B.P., et al. (2015). High-performance probes for light and electron microscopy. Nat. Methods *12*, 568–576. https://doi.org/10.1038/nmeth.3365.

39. Livet, J., Weissman, T.A., Kang, H., Draft, R.W., Lu, J., Bennis, R.A., Sanes, J.R., and Lichtman, J.W. (2007). Transgenic strategies for combinatorial expression of fluorescent proteins in the nervous system. Nature *450*, 56–62. https://doi.org/10.1038/nature06293.

40. Maren, S., Phan, K.L., and Liberzon, I. (2013). The contextual brain: implications for fear conditioning, extinction and psychopathology. Nat. Rev. Neurosci. *14*, 417–428. https://doi.org/10.1038/nrn3492.

41. Eichenbaum, H. (2017). On the integration of space, time, and memory. Neuron *95*, 1007–1018. https://doi.org/10.1016/j.neuron.2017.06.036.

42. Pennartz, C.M.A., Ito, R., Verschure, P.F., Battaglia, F.P., and Robbins, T.W. (2011). The hippocampal-striatal axis in learning, prediction and goal-directed behavior. Trends Neurosci. *34*, 548–559. https://doi.org/10.1016/j.tins.2011.08.001.

43. Soltesz, I., and Losonczy, A. (2018). CA1 pyramidal cell diversity enabling parallel information processing in the hippocampus. Nat. Neurosci. *21*, 484–493. https://doi.org/10.1038/s41593-018-0118-0.

44. Dong, H.W., Swanson, L.W., Chen, L., Fanselow, M.S., and Toga, A.W. (2009). Genomic-anatomic evidence for distinct functional domains in hippocampal field CA1. Proc. Natl. Acad. Sci. USA *106*, 11794–11799. https://doi.org/10.1073/pnas.0812608106.

45. Voorn, P., Vanderschuren, L.J., Groenewegen, H.J., Robbins, T.W., and Pennartz, C.M.A. (2004). Putting a spin on the dorsal-ventral divide of the striatum. Trends Neurosci. *27*, 468–474. https://doi.org/10.1016/j.tins.2004.06.006.

46. Thorn, C.A., Atallah, H., Howe, M., and Graybiel, A.M. (2010). Differential dynamics of activity changes in dorsolateral and dorsomedial striatal loops during learning. Neuron *66*, 781–795. https://doi.org/10.1016/j.neuron.2010.04.036.

47. Belin, D., and Everitt, B.J. (2008). Cocaine seeking habits depend upon dopamine-dependent serial connectivity linking the ventral with the dorsal striatum. Neuron *57*, 432–441. https://doi.org/10.1016/j.neuron.2007.12.019.

48. McGeorge, A.J., and Faull, R.L. (1989). The organization of the projection from the cerebral cortex to the striatum in the rat. Neuroscience *29*, 503–537. https://doi.org/10.1016/0306-4522(89)90128-0.

49. Brog, J.S., Salyapongse, A., Deutch, A.Y., and Zahm, D.S. (1993). The patterns of afferent innervation of the core and shell in the "accumbens" part of the rat ventral striatum: immunohistochemical detection of retrogradely transported fluoro-gold. J. Comp. Neurol. *338*, 255–278. https://doi.org/10.1002/cne.903380209.

50. Kelley, A.E., and Domesick, V.B. (1982). The distribution of the projection from the hippocampal formation to the nucleus accumbens in the rat: an anterograde- and retrograde-horseradish peroxidase study. Neuroscience *7*, 2321–2335. https://doi.org/10.1016/0306-4522(82)90198-1.

51. Groenewegen, H.J., Vermeulen-Van der Zee, E., te Kortschot, A., and Witter, M.P. (1987). Organization of the projections from the subiculum to the ventral striatum in the rat. A study using anterograde transport of Phaseolus vulgaris leucoagglutinin. Neuroscience *23*, 103–120. https://doi.org/10.1016/0306-4522(87)90275-2.

52. Groenewegen, H.J., Room, P., Witter, M.P., and Lohman, A.H. (1982). Cortical afferents of the nucleus accumbens in the cat, studied with anterograde and retrograde transport techniques. Neuroscience *7*, 977–996. https://doi.org/10.1016/0306-4522(82)90055-0.

53. Trouche, S., Koren, V., Doig, N.M., Ellender, T.J., El-Gaby, M., Lopes-Dos-Santos, V., Reeve, H.M., Perestenko, P.V., Garas, F.N., Magill, P.J., et al. (2019). A hippocampus-accumbens tripartite neuronal motif guides appetitive memory in space. Cell *176*, 1393–1406.e16. https://doi.org/10.1016/j.cell.2018.12.037.

54. Crombag, H.S., Bossert, J.M., Koya, E., and Shaham, Y. (2008). Review. Context-induced relapse to drug seeking: a review. Philos. Trans. R. Soc. Lond. B Biol. Sci. *363*, 3233–3243. https://doi.org/10.1098/rstb.2008.0090.

55. Lieberman, J.A., Girgis, R.R., Brucato, G., Moore, H., Provenzano, F., Kegeles, L., Javitt, D., Kantrowitz, J., Wall, M.M., Corcoran, C.M., et al. (2018). Hippocampal dysfunction in the pathophysiology of schizophrenia: a selective review and hypothesis for early detection and intervention. Mol. Psychiatr. *23*, 1764–1772. https://doi.org/10.1038/mp.2017.249.

56. Martin, L., Stein, K., Kubera, K., Troje, N.F., and Fuchs, T. (2022). Movement markers of schizophrenia: a detailed analysis of patients' gait patterns. Eur. Arch. Psychiatr. Clin. Neurosci. *272*, 1347–1364. https://doi.org/10.1007/s00406-022-01402-y.

57. Zolotukhin, S., Byrne, B.J., Mason, E., Zolotukhin, I., Potter, M., Chesnut, K., Summerford, C., Samulski, R.J., and Muzyczka, N. (1999). Recombinant adeno-associated virus purification using novel methods improves infectious titer and yield. Gene Ther. *6*, 973–985. https://doi.org/10.1038/sj.gt.3300938.

STAR★METHODS

KEY RESOURCES TABLE

REAGENT or RESOURCE	SOURCE	IDENTIFIER
Bacterial and Virus Strains		
pRC-DJ	Dr. Mark Kay lab, Stanford Univ.	N/A
AAV-tTA	Li et al., 2021[23]	Addgene, Plasmid #175280
AAV-rtTA	Li et al., 2021[23]	Addgene, Plasmid #175274
AAV-TRE-IEo	This paper	GenBank: OQ923270; Addgene: Plasmid #201992
AAV-IE180^{WT}	This paper	N/A
AAV-DIO-EGFP	Xu et al., 2013	AAV-dfi-EGFP
pRC-rAAV2-retro	Tervo et al., 2016[34]	Addgene 81070
PRV154	Center for Neuroanatomy with Neurotropic Viruses (CNNV)	PRV154
PRV$^{\Delta IE}$-Cre (IE180 null Becker with Syn-Cre in Us9Loci)	Oyibo et al., 2014[17]; Dr. Anthony Zador's lab at Cold Spring Harbor Laboratory	
PRV$^{\Delta IE}$-EGFP (IE180 null Becker with EF1a-GFP in Us9 Loci)	Dr. Anthony Zador's lab at Cold Spring Harbor Laboratory	PRV128
Chemicals, Peptides, and Recombinant Proteins		
Doxycycline hyclate	MP Biomedicals	219895501
Deposited Data		
AAV-TRE-IEo	This paper	GenBank: OQ923270
Raw data of images of brain sections	This paper	https://doi.org/10.5281/zenodo.7941542
Experimental Models: Cell Lines		
293T cell	ATCC	CRL-3216
3T3 cell	ATCC	93061524
BHK cells	ATCC	CCL-10
Pk15-IE180 cell	Dr. Lynn W. Enquist lab, Princeton Univ.	N/A
Experimental Models: Organisms/Strains		
Mouse: Ai9	The Jackson Laboratory	007909

RESOURCE AVAILABILITY

Lead contact
Further information and requests for resources and reagents should be directed to and will be fulfilled by the lead contact, Wei Xu (wei.xu1@utsouthwestern.edu).

Materials availability
The sequence of the AAV plasmid generated in this study, pAAV-TRE-IEo, has been deposited to GenBank : OQ923270. The plasmid has been deposited to Addgene (plasmid #201992). Raw data of images of brain sections have been deposited to https://doi.org/10.5281/zenodo.7941542. Other reagents reported in this paper are available from the lead contact upon request.

Data and code availability
- The raw data of microscopic images of brain sections have been deposited to Zenodo and are publicly available as of the date of publication. The DOI is listed in the key resources table. All data reported in this paper will also be shared by the lead contact upon request.
- This paper does not report original code.
- Any additional information required to reanalyze the data reported in this paper is available from the lead contact upon request.

EXPERIMENTAL MODEL AND STUDY PARTICIPANT DETAILS

Mice

6-15 weeks old Ai9 mice (JAX stock No. 007909), were group housed on a 12 h light/12 h dark cycle with *ad libitum* access to food and water. Since literature does not show a difference of animals' sex in PRV tracing, the sex of the mice was not accounted for in this study. Male and female mice were randomly assigned to experimental groups. Animal work was approved and conducted under the oversight of the UT Southwestern Institutional Animal Care and Use Committee and complied with Guide for the Care and Use of Laboratory Animals by National Research Council.

Cell culture

293T cells, 3T3 cells, BHK cells and Pk15-IE180 cells were used to generate AAV, test PRV replication and amplification of PRV$^{\Delta IE}$, respectively. 293T, 3T3 and BHK cells were grown in Dulbecco's Modified Eagle's Medium (DMEM) containing 10% Fetal Bovine Serum (FBS). Pk15-IE180 cells were grown in DMEM containing 10% FBS and 700 μg/mL of G-418. The replication of PRV$^{\Delta IE}$ was tested in two distinct cell lines (3T3 cells and BHK cells).

METHOD DETAILS

Viral vector construction

AAV vectors were constructed with AAV2 inverted terminal repeats (ITRs). In AAV-TRE-IE^{WT} and AAV-IEo, the following components were arranged sequentially downstream of left-ITR: the tetracycline-responsive element and a minimal CMV promoter, the coding sequence of wild-type IE180 or IEo, a minimal SV40 poly A sequence, and the right ITR. The coding sequence of IEo is:

ATGGCTGACGACTTGTTCGACTTTATCGAAACCGAGGGAAACTTTTCACAGCTTCTTGCAGCAGCTGCCGCAGCAGCAGAGGAG
GAAGGTATCGCAAGTGGACCCGACGGTGGTAGTCAGGGGTCAAGGCGCCGCGGATCTTCAGGTGAGGACCTGCTGTTTGGTCCT
GGAGGATTGTTTAGTGATGATGCTGCAGAGGCAGAAGCTGAGGCCGCCGTGCTCGCCGCAGCCGCTGGCGCTACACGGCCCCC
CCGACCTCCCAGTGCTCAGCAACAGCAGCCTCGCCGAGGTTCAGGTGAGATTGTCGTTCTCGACGATGAGGATGAAGAAGAAGA
TGAGCCTGGCAGCCCCGCTGCTGGAAGTCCAGGACGAGCCTTGCATCAAGGGTCCGAACATGGGCATCTTGTGCTTGGTCCTAG
AAGCCGAGCAGGGAGTGGCCCCAGACCACCCACACCCGCCGCTCTTGCTGCCGCTGAGGCAGGTGCCCCTGGGGGCCCCGGC
AGGAGCAGCCCTTCTGCTGCTTCCCCAGCCAGTTCCAGCGGCTCACCTGGCCCATCCGCCGCCCCAAGGCGATGGAGTCCTGC
CGGCGATCCTGTTGGAGAACCTGGTCCAGCCGCCAGACCAAGAACCCCCGCTCCTCCTGCTCAGCCTGCCGCAGTTGCTGCAG
CTCCAGCACGACGCGGACCAGCCTCACCAGCACCTCCTGCCGCAGGACCAGTTAGCGCTCCAGGTGGAGGAGGTGCACCCAGC
GCCGGTGGAGACAGAGGTCGCCACCACCACCAGCATAGGGAACCTCTTTTGGACGAACCCGCCGCAGCCAGACGGTTGGACCC
CAGGCCACTTGGTGCAAGGTCCCCTGTCTCATCAAACCCCAATTCAAACTCCTCCAGCACCACAACTGTAGCAGTTGAGCCAGTCG
CTAGGGGGCCCGAGAAGGATGAAGATGGACTGGGTCCCGCCGGGGATGGAGGGGCACCTCCACAACGACAGCCCAGGCGACG
GCGAGCCGGCGAAGGAGCATTGAGAAGGGGACGAGGATTTAGCAGTTCAAGCAGCGGAGGGAGCGACTCTGACCTGAGTCCCGC
TAGGTCCCCAAGCGCCCCCCGCGCTCTGGCTGCTGCTGCTGCTAGGCGAAGTGCTTCCAGTAGCTCAAGCTCCTCATCCTCCAGT
TCTAGCTCTAGTTCTTCAGAAGGCGAGGAAGACGAAGGTGTTAGGCCTGGTGCCCCACTGGCACGAGCAGGACCACCACCATCT
CCCCCTGCACCTGCCGCCGCACCTAGACCTAGCGCCTCCTCTGCCTCTAGTAGTGCCGCAGCCAGCCCTGCCCCCGCACCCGA
ACCTGCCCGACCCCCTCGCAGAAAGAGACGATCAACAAATAACCATCTTTCATTGATGGCCGATGGACCACCTCCAACTGACGGA
CCATTGCTTACCCCACTGGGTGAGCCTTGGCCAGGGTCTGATCCCCCAGCAGACGGCCGCGTCCGGTACGGGGGTGCCGGCGA
TTCCCGCGAAGGACTCTGGGACGAAGACGATGTACGCCAAGCAGCTGCCCGCTATCGCGCCGCCGCAGGACCCGTTCCCGTGTT
CATTCCTGAGATGGGCGATTCACGGAAACAACACGAAGCCCTTGTAAGACTCATTTACTCTGGTGCAGCAGGAGAAGCAATGTCTTG
GCTCCAAAATCCCAGAATGCAAGCTCCCGACCAACGATTCAACCAGTTCTGTCAAAGAAGAGTGCATGCACCCCATGGGCACGGA
AGCTTTATCACTGGAAGCGTTACTCCCCCTCTGCCACATATAGGTGACGCTATGGCAGCACAAGACCCACTGTGGGCTCTGCCCCA
TGCTGTGTCTGCAGTTGCCATGTCCCGCCGGTAAGAGCCGCAGATCCTCGGGCCGGTGAAGCCACTGTAGAGGCCCTGTGCGCC
AGGGTTCGGGCCGCTTTCGCAGCAGCCCAGCCAGGCCGGGTTCCACGAGAATTGGCTGATGCTTGCGTACTTGCATGCCGCGGT
GTACTCGAACGCTTGCTTCCCTGCCCCTTGCGCCTGCCAGCACCTGCCAGAGCTCCTGCTGCCCTGGGGCCCGCATGTTTGGAG
GAAGTCACCGCTGCTCTTCTGGCACTCAGAGATGCTATCCCCGGAGCCGGCCCTGCAGAACGACAACAAGCTGCAGACGCAGTAG
CACTCGTAGCAAGAACCGTTGCCCCCCTGGTTCGATATTCCGTAGATGGTGCTCGGGCTCGCGAAGCTGCTTGGACCTACGCCG
CTGCATTGTTCGCCCCTGCAAATGTCGCTGCTGCAAGACTGGCTGAAGCTGCCGCTCGGCCAGGTCCCGCCGAACCTGCCCCTG
GCCTCCCCCCACTTTGGCCCGAACAACCCGGGTTGGTCGTGCCAGCTCCTGCACCTGCTGCAGCTGGCGCTCCCAGTGGATTGC
CCGGCTCCGGTCCTAGTTCACCAGCCTCTACTAAAAGTTCAAGCTCAACCGAGTCCGGGAGCAGCACCAAGTCATCTTCCGGGA
CCAAATCTGGCCTGAGTGGCTCTTCTGGTTACGCTTCCAGTCCTGCAGCAGGGCCAGACCCCGCCCCTGAACGGCGCAAAAAGA
AGAGACGAGCACCCGGAGCACGGCGACCCGGGGACGGTGAAGAGGATGAAGGGCTCTCTGGTGCCGCCCTCCGCGGCGACGG
CCACGGTCATAGGGACGATGAGGAGGATCGCGGCCCTAGACGGAAACGGAGAAGTCTGGGGCTTGGTCCAGCACCCGACCCCG
CACCAGCTCTGCTCAGCAGTAGCAGCTCATCCGAAGACGACAGATTGCGACGGCCCCTCGGACCTATGCCTGAACATCCTGCTCC
AGACGGCGGTTTCCGAAGAGTACCAGCCGGGGAGACTCATACTCCTAGACCTAGCGAAGCCGCCCTTGCAGCATATTGTCCCCCT
GAGGTAGCTAGAGCTTTGGTGGACCAAGAGGTTTTTCCCGAGCTGTGGCGCCCTGCTCTTACATTTGACCCCGCTGCCCTCGCTCA
CATCGCTGCTCGGCGCGGGAGCTGCCGGCGCTCCTTTGCGACGGAGAGCTGCATGGATGCGCCAAATCGCCGACCCCGAAGACG

TTCGAGTTGTCGTCCTTTACGACCCCCTGCCCCATGAGGAACTTTGCGCAGAGCCTGCTGAAGGCGCCCCAAGGCCAGCTTGGG
ATCCTAGACGAGGTGGCCTTTCCGCTCTGCTTGCAGCATTTGCTCACCGGCTGTGCACTCCAGATTCCCACGCTTGGGCAGGAAA
TTGGACTGGGAGACCCGATATCGGTCGGTTGAATGCCCAAGGTGTACTCCTCTTGTCTGCTCGCGACCTCGGATTTGCAGGCGCA
GTGGAGTATCTCTGCTCTCGCCTGGGAGCAGCTAGGCGGAGGCTTATTGTTCTTGACACTATTGAAGATTGGCCTGCAGACGGGC
CCGCCGTCGGGGATTACCATGTGTACGTTCGCGCCAGGTTGGATCCCGCCGCCCAGTGCGCTGTACGATGGCCCGGATGCAGG
GAACTTAGGGCTGCCGTGTTGGACTCTAGTTCAATCGTTGGTCCTGCATGCTTTGCTCGAGCAGAGGCTTCATTTGCAAGGTTGCA
CCCCGGCGCCGAACCCTTGAGACTCTGCCGACAGGACAATGTGCGGTACACTGTATCTACACGAGCAGGGCCACGGACACCTG
TTCCTCTTCCCCCAAGAGCATACCGCCAACGGGTACTCCCTACAGTAGACGGATGTAAGGACATGGCTCGCCAGCGCTCAGCTT
TGGGACTCGGCGACCCCGACTTCGACGCTGGAGCAGCCTTCGGTCATCGGGCAGCCAACAGGTGGGGGCTCGGGGCCCCATTG
CGCCCTGTCTTCGTGTCCTGTGGAAGAAGGGGGCTGGCAGAATTGCGCGGCCCAGAGGGCCTTCCAGCCGAGTTGCGGGCCTT
TTGTGCCGCTGCCCTCCTTGAGCCTGATGCCGAAGCAGCTCCCTTGGTGCTCACCCCCGGGGCCGTAGCTGCAGCCGGTGCACC
TCCAGCTGTCTTGTGGGATTTTGCCCCATTTGAAACTTCCGTTCGAGCAGCAGCTGGGGGAGCCGTGGAAACTCGACGCCCCGCA
GGGGCTTCAGGGGCCGGCGCCGGACCAGGAGAAGATGGTGATTCTGTTGAGATTGTCGGGGTGCGGGGTGGGGACGGACGACC
ACGGGGGCCCCTCGGACCAATTAAGGTTGAGGCAATCTCTGACGATGAAGAAGCAGAAGATGCTGGCAACCCTTACCTTCTTCTG
CGCTAA.

Virus production

All AAVs except rAAV2-*retro*-tTA were packaged with AAV-DJ capsids. AAV2-*retro*-tTA was packaged with rAAV2-retro capsid genes (rAAV2-retro helper plasmid, Addgene 81070). Virus was prepared as described.[57] Briefly, the AAV expression plasmids were co-transfected with pHelper and pRC-DJ (for AAV-DJ), or pHelper and rAAV2-retro helper plasmid (for rAAV2-retro) into 293T cells. Cells were collected 72 h later, lysed, and loaded onto iodixanol gradient for centrifugation at 400,000 g for 2 h. The fraction with 40% iodixanol of the gradient was collected, washed, and concentrated with 100,000 MWCO tube filter. The genomic titer of virus was measured with quantitative real-time PCR. The titers of AAVs used for stereotaxic intracranial injection were in the range of 1–2 x 10^{13} copies/ml. AAV-tTA (or AAV-rtTA) was mixed with AAV-TRE-IEo (or AAV-TRE-IE^{WT}) at 1:1 ratio for stereotaxic injections. For infection of cultured cells, 2.0 X 10^9 genomic copies of AAV-tTA (or AAV-rtTA) and AAV-TRE-IEo (or AAV-TRE-IE^{WT}) were added to each well in 24-well culture plates (containing 0.5 mL of cell culture medium/well).

PRV$^{\Delta IE}$ was amplified by infecting Pk15-IE180 cells, which express wild-type IE180 under the control of Dox, as described.[17] Briefly, Pk15-IE180 cells were infected with a stock of IE180-null PRV in the presence of 1 μg/mL of Dox (MP Biomedical, 219895501). 3–4 days later, the infected cells, after showing apparent cytopathic effect, were collected and lysed by three freeze-thaw cycles followed by sonication. Cell lysate was clarified by centrifuge for 10 min at 3000 g. The supernatant was laid on top of a sorbitol buffer and centrifuged for 2 h at 4°C at 23.5k rpm with an SW28 rotor. The pellet was suspended in DMEM. PRV$^{\Delta IE}$ were titered by plaque-forming assay on Pk15-IE180 cells in the presence of 1 μg/mL of Dox. The titers were: PRV$^{\Delta IE}$-Cre 3.75 E+08 pfu/mL, PRV$^{\Delta IE}$-EGFP 5.15 E+08 pfu/mL. The titer of PRV154 from CNNV core was 4.05E+08 pfu/mL. To infect 3T3 cells (Figure 1), 3.0 × 10^2 PFU of PRV$^{\Delta IE}$-EGFP was added to each well in 24-well culture plates.

Stereotaxic viral injection

Mice were anesthetized with tribromoethanol (125–250 mg/kg) or isoflurane inhalation (1.5–2%). Viral solution was injected with a glass pipette at a flow rate of 0.10 μL/min. After the completion of injection, the glass pipette was left in place for 5 min before being retrieved slowly. The coordinates for each of the injection sites on the anterior-posterior direction from the bregma (AP), medial-lateral direction from the midline, and the dorsal-ventral direction from the dura (DV) are listed in the format: Region (AP, ML, DV). On the AP direction, "+" denotes anterior to the bregma and "-" denotes posterior to bregma. The coordinates are as the following: dorsal CA1 (−1.95, 1.35,1.20); ventral CA1(-3.00, 3.50, 5.00); dorsal CA3 (−2.25, 2.75, 2.50); DG (−2.00, 1.25, 2.20); dSUB (−3.15, 2.00, 1.75); LS (+0.55, 0.45, 2.70); PFC (+1.25, 0.30, 1.25); dorsal striatum (+0.55, 1.65, 3.00); NAc (+1.00, 1.10, 5.20); rRSP (−2.25, 0.25, 0.75); SNr (−3.15, 1.15, 5.50); SUM (−2.50, 0.00, 5.75); and EC (−4.80, 3.60, 2.60). We injected between 0.25 and 0.5 μL of AAV viral solution, or 0.5 μL of PRV solution, at each injection site unless stated otherwise. The injections were unilateral.

Doxycycline administration

In this study, we tested three ways of administering doxycycline (Dox): intraperitoneal injection (50 mg/kg body weight, dissolved in prewarmed saline), feeding with Dox diet (containing doxycycline hyclate, 625 mg/kg diet), or through drinking water (200 μg/mL with 1% sucrose). Dox diet caused minimal disturbance to the mice and we preferred it, while intraperitoneal injection provided the most accurate temporal control.

Histological analysis

Under deep anesthesia with isoflurane inhalation, mice were transcardially perfused with 10 mL of PBS followed by 40 mL of 4% paraformaldehyde (PFA) in PBS. The brains were extracted and postfixed overnight in 4% PFA at 4°C, and cryoprotected in 30% sucrose. Brains were sectioned with a cryostat to a thickness of 40-μm. Free-floating sections were washed in PBS, mounted on glass slides and sealed with antifade mounting medium. All fluorescent signal in this study was from native EGFP or tdTomato without immunostaining. The whole-mount brain sections were scanned with Zeiss AxioscanZ1 digital slide scanner with a 10× objective.

The high-resolution images were taken with ZEISS LSM 880 confocal microscope. To quantify tdTomato-positive cells in the coronal sections, we used the following rules to determine the borders between the hippocampal subregions: (1) The dorsal and ventral DG are demarcated at the horizontal line at the level of the dorsal edge of the rhinal fissure (Line A). (2) The dorsal and intermediate CA1 (or CA3) are demarcated at a horizontal line at the level of the ventral edge of the lateral blade (suprapyramidal blade) of the dorsal dentate gyrus (Line B). (3) The intermediate and ventral CA1 (or CA3) are demarcated at Line A. (4) In the caudal sections where Line B is at the same level or below—ventral to–Line A, the CA1 (or CA3) above line A is considered intermediate CA1 (or CA3), and those below Line A is considered ventral CA1 (or CA3). Cell densities in Figure 2D were calculated by dividing the number of tdTomato-positive cells by the area of the granule cell layer. To compare the pathways, the cell densities in Figures 6 and 7 were calculated by dividing the number of tdTomato-positive cells by the area of the hippocampal subregion (e.g. dorsal CA1, dorsal DG, etc.).

Brain slice electrophysiology recording

3 weeks after PRV$^{\Delta IE}$-cre injection in CA1, transverse slices of the dorsal hippocampus (with a thickness of 300 μm) were prepared with a vibratome (Leica VT1200) in ice-cold cutting solution containing (in mM): 2.5 KCl, 1.2 NaH$_2$PO$_4$, 26 NaHCO$_3$, 10 D-glucose, 213 sucrose, 5 MgCl$_2$, 0.5 CaCl$_2$. The slices were incubated in cutting solution for 30 min at 32°C and then in artificial cerebrospinal fluid (ACSF) containing (in mM): 124 NaCl, 5 KCl, 1.2 NaH$_2$PO$_4$, 26 NaHCO$_3$, 10 D-glucose, 1 MgCl$_2$, 2 CaCl$_2$ for at least 1 h at 32°C. The cutting solution and ACSF were adjusted to pH 7.3–7.4 and 290–300 mOsm and constantly aerated with 95% O$_2$/5% CO$_2$. Whole-cell patch clamp recording was performed in a recording chamber perfused (~1 mL/min) with oxygenated ACSF at 26–28°C. The recording pipettes (2–4 MΩ) were filled with internal solution containing (in mM): 125 K-gluconate, 20 KCl, 4 Mg-ATP, 0.3 Na-GTP, 10 Na$_2$-phosphocreatine, 0.5 EGTA, 10 HEPES, adjusted to pH 7.3–7.4 and 310 mOsm. Post-synaptic currents were recorded in voltage-clamp mode with holding potential at −70 mv. The resting potentials and current injection-induced action potentials were recorded in current-clamp mode.

QUANTIFICATION AND STATISTICAL ANALYSIS

Data are presented as mean ± standard error of the mean (SEM). Sample number (n) indicates the number of cells or mice in each experiment and is specified in the figure legends. Statistical significance was analyzed with Mann-Whitney test. p < 0.05 is considered statistically significant.